NONLINEAR DYNAMICS OF FUNCTIONALLY GRADED ROTATING BEAMS UNDER THERMOELASTIC TRANSVERSE LOADING

Sebastián P. Machado, smachado@frbb.utn.edu.ar
Marcelo T. Piovan, mpiovan@frbb.utn.edu.ar
Grupo Análisis de Sistemas Mecánicos, Centro de Investigaciones de Mecánica Teórica y Aplica, Universidad Tecnológica Nacional FRBB. 11 de Abril 461, B8000LMI, Bahía Blanca. Argentina.

Abstract. *Strategic and high technology industries, such as defense, aerospace or automotive industries are demanding new and advanced materials in order to improve the structural response as well as to enhance their endurance. This is particularly true in the case of rotating blades that are subjected to severe environmental conditions such as high temperatures as well as mechanical conditions such as high rotating accelerations, centrifugal forces, geometric stiffening, among others. It is well known that flexible beams become stiffer when subjected to high speed rotations, because of the nonlinear geometrical coupling associated to the large displacements of the beam cross-section. In this work, an analysis is performed on the nonlinear planar vibrations of a functionally graded beam subjected to a combined thermal and harmonic transverse load in the presence of internal resonance. Adopting the direct perturbation MMS technique, the partial differential equations of motion of the beam are reduced to sets of first-order nonlinear modulation equations in terms of the complex modes of the beam. The assumption of steady-state values of centrifugal loads is evaluated. It has to be said that there is a lack of information about modeling of rotating beams made of FGM under severe thermo-mechanical loads. This paper is intended to be a contribution on the subject.*

Keywords*: Nonlinear dynamics, FGM, Internal Resonance*

1. INTRODUCTION

Vibrations of rotating blades or beams have been a subject of constant research interest since they are applied in the design of helicopter blades, turbopropeller blades, wind-turbine blades and robotic arms. The most simplified representation of a rotating beam is a one-dimensional Euler-Bernoulli model. A uniform rotating beam of doubly symmetric cross-section is a special case (no torsional motion: i.e., out-of-plane (flapping) vibration and in-plane (lead-lag) vibration are uncoupled). Owing to the stiffening effect of the centrifugal tension, one can expect the natural frequencies to increase with an increase in the speed of rotation. In several publications a cantilever beam under rotating speed has been considered and approximate methods such as Rayleigh-Ritz, Galerkin, finite element methods, etc., has been used to derive natural frequencies (Schilhansl, 1958; Leissa, 1981). However, the nonlinear dynamic analysis of rotating beam is rather rare in the literature (Pesheck *et al*. 2002a and b; Apiwattanalunggarn *et al*. 2003; Ozgur and Gokhan, 2009). Systematic procedures have been developed to obtain reduced-order models (ROMs) via nonlinear normal modes (NNMs) that are based on invariant manifolds in the state space of nonlinear systems (Shaw and Pierre 1993, 1994; Shaw *et al*., 1999). These procedures initially used asymptotic series to approximate the geometry of the invariant manifold and have been used to study the nonlinear rotating Euler–Bernoulli beam (Pesheck *et al.*, 2002a). Pesheck *et al*. 2002b, employed a numerically-based Galerkin approach to obtain the geometry of the NNM invariant manifolds out to large amplitudes. These procedures can be applied to more general nonlinearities over wider amplitude ranges, and have been applied to study the vibrations of a rotating Euler–Bernoulli beam (Pesheck *et al*., 2001). Apiwattanalunggarn *et al*. (2003) presented a nonlinear one-dimensional finite-element model representing the axial and transverse motions of a cantilevered rotating beam, which is reduced to a single nonlinear normal mode using invariant manifold techniques. They used their approach to study the dynamic characteristics of the finite element model over a wide range of vibration amplitudes. As it can be note, the interest of most of works about nonlinear dynamic of rotating beams are focus on the reduced-order model as the invariant manifold solution. Turhan and Bulut (2009) investigated the in plane nonlinear vibrations of a rotating beam via single- and two-degree-of-freedom models obtained through Galerkin discretization. They performed a perturbation analyses on single- and two-degree-of-freedom models to obtain amplitude dependent natural frequencies and frequency responses. In the last four references, the computational cost associated with generating the manifold solution and the efficiency of the resultant model was mainly analyzed.

From the review of literature, it is found that the study of internal resonance in the area of cantilever rotating slender beam subjected to a harmonic transverse load has not yet been explored so far, neither in the context of composite materials nor in the context of functionally graded materials. The nonlinear modal interaction or the internal resonance in the system arising out of commensurable relationships of frequencies, in presence of parametric excitation due to periodic load can have possible influence on system behavior, which needs to be studied.

In the present paper, we analyze the nonlinear planar vibration of a rotating cantilever FGM beam with harmonic transverse load in the presence of internal resonance. The model is based on one-dimensional Euler-Bernoulli formulation where the geometric cubic nonlinear terms are included in the equation of motion due to midline stretching of the beam. The linear frequencies of the system are dependent on the rotation speed and this effect is used to activate the internal resonance. For a particular rotation speed the second natural frequency is approximately three times the first natural frequency and hence the first and second modes may interact due to a three-one internal resonance. For a comprehensive review of nonlinear modal interactions, we refer the reader to Nayfeh and Mook (1979), and Nayfeh (1996). The method of multiple scales (MMS) is used to attack directly the governing nonlinear partial differential equation of motion of the beam and reduced the problem to sets of first-order nonlinear modulation equations in terms of the complex modes of the beam. These modulation equations are numerically analyzed for stability and bifurcations of trivial and nontrivial solutions. The trivial state stability plots are presented. The modulation equations are also numerically integrated to obtain the dynamic solutions periodic, quasiperiodic and chaotic responses for typical system parameters.

2. FUNCIONALLY GRADED MATERIAL AND ITS THERMAL PROPERTIES

The laws of variation of the material properties along the wall thickness can be prescribed in order to bear in mind for different types of material gradation such as metal to ceramic or metal to metal (e.g. steel and aluminium). Functionally graded shells are usually considered to be composed by many isotropic homogeneous layers (Tanigawa, 1995). In this case, a simple gradation based in a power-law is employed. The law of variation of the elastic and mass properties along the wall-thickness *e* is:

$$\mathcal{P}\left(n\right)=\mathcal{P}_M+\left(\mathcal{P}_C-\mathcal{P}_M\right)\left(\frac{2n+e}{2e}\right)^K , \tag{1}$$

where, $\mathcal{P}(n)$ denotes a typical material property (i.e., density ρ or Young's modulus E or Poisson coefficient ν). Sub-indexes C and M define the properties of the material of the outer surface (normally ceramic) and inner surface (normally metallic), respectively. The exponent K, which is connected to the ratio of constituents in volume, can have different values that may vary between zero (i.e., a full ceramic phase) or infinity (i.e., a full metallic phase).

It is assumed that the beam is subjected to a steady-state one dimensional (1-D) temperature distribution through its thickness. The steady-state 1-D heat transfer equation is expressed by:

$$\frac{\mathrm{d}}{\mathrm{d}n}\left[k(n)\frac{\mathrm{d}T}{\mathrm{d}n}\right]=0 , \tag{2}$$

where k is the coefficient of the thermal conduction. The boundary conditions are:

$$T=T_M \quad \text{at} \quad n=-\frac{e}{2} \quad \text{and} \quad T=T_C \quad \text{at} \quad n=\frac{e}{2}. \tag{3}$$

The solution of Eq. (4) can be obtained by means of the polynomial series. Therefore, $T(n)$ is calculated as (Zhao *et al*. 2007):

$$T\left(n\right)=T_M+\frac{\Delta T}{\sum_{j=0}^{\psi}(-1)^j\frac{\left(k_C-k_M\right)^j}{\left(1+jK\right)k_M^j}}\sum_{j=0}^{\psi}(-1)^j\frac{\left(k_C-k_M\right)^j}{\left(1+jK\right)k_M^j}\left(\frac{n}{e}+\frac{1}{2}\right)^{(1+jK)} \tag{4}$$

where, normally the upper limit of the summation is $\Psi \rightarrow \infty$, however by means of an elemental numerical study one can prove that Eq. (4) may be finely approximated by taking just a few terms, or more practically, $\Psi \geq 5$ as it was done by many researchers (Malekzadeh, 2009).

Throughout the numerical simulation T_M is taken 300 K. It is assumed that the properties of the FGM are temperature-dependent and vary according to a law obtained experimentally. These are expressed in a general form as (Reddy and Chin, 1998):

$$p\left(n\right)=p_0\left(p_{-1}/T+1+p_1T+p_2T^2+p_3T^3\right), \tag{5}$$

in which p is a temperature-varying material property in general (i.e. modulus of elasticity, or Poisson's coefficient, etc.), T is the absolute temperature [^oK] and the coefficients p_i are unique for a particular material and obtained by means of a curve fitting procedure. Thus the material properties can be represented as a function of the thickness and the temperature. It is clear that p_0 is the typical material property in absence of thermal effects.

3. NON-LINEAR EQUATIONS OF MOTION

We consider the dynamic response of a rotating box beam subjected to harmonic transverse loads (see Fig. 1). The origin of the beam coordinate system (x, y, z) is located at the blade root at an offset R_0 from the rotation axis fixed in space. R_0 denotes the radius of the hub (considered to be rigid) in which the blade or beam is mounted and which rotates about its polar axis through the origin *0*. We assume that the motion is planar and the cross sections remains plane during transverse bending. A doubly symmetric cross-section box-beam is used and so out-of-plane (flapping) and in-plane (lead-lag) vibration are uncoupled. Neglecting rotary inertia and the transverse shear, the non-linear equations of motion of a rotating beam yields (Machado *et al*. 2007; Librescu, 2006):

$$\rho A\,\ddot{u} - N' - \rho A\left(R_0 + x + u\right)\Omega^2 = 0\,, \tag{6}$$

$$EI\ v^{iv} - \left(N\ v'\right)' + \rho A\,\ddot{v} = F(x)\cos(\varpi t)\,, \tag{7}$$

where N is axial beam force,

$$N = EA\left(u' + \frac{1}{2}v'^2 - \bar{Q}_T\right), \tag{8}$$

Ω is the beam rotation speed, ρA is the mass per unit length, EA and EI are the axial and flexural rigidity, ϖ is the excitation frequency, $F(x)$ describes the spatial distribution of the applied transverse harmonic load, and $\bar{Q}_T = \alpha\,\Delta T$. Overdots indicate differentiation with respect to time and primes with respect to the axial co-ordinate.

Substituting the axial beam force from Eq. (8) into Eq. (7) and neglecting the inertial effects along the longitudinal direction, the non-linear equations of motion of a rotating beam yields:

$$\rho A\,\ddot{v} + EI\ v^{iv} - \left[\frac{EA}{2L}\int_0^L v'^2 \mathrm{dx} + \frac{\Omega^2 \rho A}{2}\left(\frac{L^2}{3} - x^2\right)\right]v'' + \rho A \Omega^2 v' x = F(x)\cos(\varpi t)\,. \tag{9}$$

Finally, introducing a nondimensional quantities $t^* = \sqrt{\dfrac{EI}{L^4 \rho A}}\,t$, $x^* = \dfrac{x}{L}$, adding damping $\mu(x)$ and dropping the asterisk, the Eq. (9) with the corresponding boundary conditions can be conveniently rewritten as:

$$\ddot{v} - \chi v'' + v^{iv} + 2\mu(x)\dot{v} - \gamma v''\int_0^1 v'^2 \mathrm{dx} + \lambda v' = f\cos(\varpi t), \qquad BC\ \begin{cases} v = 0 \ \text{ and } \ v' = 0 \ \text{ at } x = 0 \\ v'' = 0 \ \text{ and } \ v''' = 0 \ \text{ at } x = 1 \end{cases}, \tag{10}$$

where $\chi = \dfrac{\bar{N}L^2}{EI}$, $\quad \gamma = \dfrac{EA}{2EI}$, $\quad \lambda = \bar{\Omega}^2\left(\dfrac{1}{2} + \dfrac{R_0}{L}\right)$, $\quad f = \dfrac{F(x)}{EI}L^4$, $\quad \bar{\Omega}^2 = \Omega^2\dfrac{\rho A}{EI}L^4$.

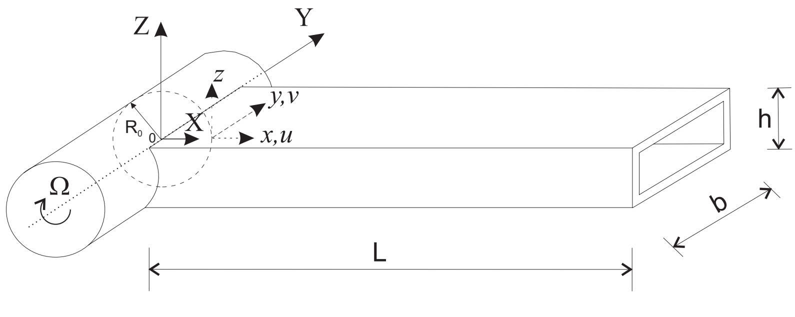

Figure 1. A schematic description of the rotating box beam.

4. METHOD OF ANALISIS

In this section, the asymptotic method of multiple scales is applied directly to the partial differential and the associated boundary conditions Eq. (10). We seek an approximate solution to this weakly nonlinear distributed parameter system in the form of a first-order uniform expansion and introduce the time scale $T_n = \varepsilon^n t$, $n = 0,1,2,...$ A small parameter ε is introduced by ordering the linear damping and load amplitude as $\mu = \varepsilon\tilde{\mu}, f = \varepsilon\tilde{f}$. Moreover, the displacement $v(x,t)$ are expanded as:

$$v(x,t) = v_1(T_0,T_1,x) + \varepsilon\ v_2(T_0,T_1,x) + ... \tag{11}$$

Substituting Eq. (4) into Eq. (2) and equating coefficients of like powers of ε on both sides, we obtain

Order ε^0:
$$D_0^2 v_1 + \alpha v_1^{iv} - \chi v_1'' + \lambda v_1' = 0\,, \tag{12}$$

Order ε^1:
$$D_0^2 v_2 + \alpha v_2^{iv} - \chi v_2'' + \lambda v_2' = -2D_0 D_1 v_1 - 2\mu(x) D_0 v_1 - \gamma v_1'' \int_0^1 v_1'^2 \mathrm{dx} + f\cos(\varpi t)\,, \tag{13}$$

where $D_k = \partial/\partial T_k$. In this work, principal parametric resonance of first mode considering internal resonance is analyzed, involving the first two modes. Since none of these first two modes is in internal resonance with any other mode of the beam, all other modes except the directly or indirectly excited first or second mode decay with time due to the presence of damping and the first two modes will contribute to the long term system response (Nayfeh, 1996). Hence the solution to the first-order perturbation can be expressed by:

$$v_1(T_0,T_1,x) = A_1(T_1)\phi_1(x)e^{i\omega_1 T_0} + A_2(T_1)\phi_2(x)e^{i\omega_2 T_0} + cc., \tag{14}$$

where $\phi_m(x)$ are the mode shapes of the rotating cantilever beam (see Eq. 15), *cc.* stands for the complex conjugate of the preceding terms and A_i are the unknown complex-valued functions.

$$\begin{aligned}\phi_m(x) = e^{x\beta_{4m}} &+ \Big\{ e^{x\beta_{3m}} \Big[-e^{\beta_{2m}}\beta_{2m}^2(\beta_{1m}-\beta_{4m}) + e^{\beta_{1m}}\beta_{1m}^2(\beta_{2m}-\beta_{4m}) + e^{\beta_{4m}}\beta_{4m}^2(\beta_{1m}-\beta_{2m}) \Big] \\ &+ e^{x\beta_{2m}} \Big[e^{\beta_{3m}}\beta_{3m}^2(\beta_{1m}-\beta_{4m}) - e^{\beta_{1m}}\beta_{1m}^2(\beta_{3m}-\beta_{4m}) - e^{\beta_{4m}}\beta_{4m}^2(\beta_{1m}-\beta_{3m}) \Big] \\ &+ e^{x\beta_{1m}} \Big[-e^{\beta_{3m}}\beta_{3m}^2(\beta_{2m}-\beta_{4m}) + e^{\beta_{2m}}\beta_{2m}^2(\beta_{3m}-\beta_{4m}) + e^{\beta_{4m}}\beta_{4m}^2(\beta_{2m}-\beta_{3m}) \Big] \Big\} \Big/ \Big[-e^{\beta_{2m}}\beta_{2m}^2 \\ &(\beta_{1m}-\beta_{3m}) + e^{\beta_{1m}}\beta_{1m}^2(\beta_{2m}-\beta_{3m}) + e^{\beta_{3m}}\beta_{3m}^2(\beta_{1m}-\beta_{2m}) \Big].\end{aligned} \tag{15}$$

In order to investigate the system response under internal and external resonance conditions, two detuning parameters σ_i are introduced: $\omega_2 = 3\omega_1 + \varepsilon\ \sigma_1, \quad \varpi = \omega_1 + \varepsilon\ \sigma_2$. Substituting Eq. (14) to find the solution of Eq. (13), we get

$$D_0^2 v_2 + \alpha v_2^{iv} - \chi v_2'' + \lambda v_2' = \Gamma_1(T_1,x)e^{i\omega_1 T_0} + \Gamma_2(T_1,x)e^{i(3\omega_1 T_0 + \sigma_1 T_1)} + \frac{1}{2} f\ e^{i(\omega_1 T_0 + \sigma_1 T_2)} + cc + NST, \tag{16}$$

where NST stands for terms that do not produce secular or small divisor terms. By means of the solvability condition we obtain the following complex variable modulation equations for the amplitude and phase.

$$\begin{aligned} p_1' &= -\mu_1 p_1 - \nu_1 q_1 + \gamma_{11} q_1 \left(p_1^2 + q_1^2\right) + \gamma_{12} q_1 \left(p_2^2 + q_2^2\right) - \delta_1 \left[2 p_1 q_1 p_2 - q_2 \left(p_1^2 + q_1^2\right)\right], \\ q_1' &= -\mu_1 q_1 + \nu_1 p_1 - \gamma_{11} p_1 \left(p_1^2 + q_1^2\right) - \gamma_{12} p_1 \left(p_2^2 + q_2^2\right) - \delta_1 \left[2 p_1 q_1 q_2 + p_2 \left(p_1^2 - q_1^2\right)\right] + \frac{1}{2} f_1, \\ p_2' &= -\mu_2 p_2 - \nu_2 q_2 + \gamma_{21} q_2 \left(p_1^2 + q_1^2\right) + \gamma_{22} q_2 \left(p_2^2 + q_2^2\right) + \delta_2 q_1 \left(3 p_1^2 - q_1^2\right), \\ q_2' &= -\mu_2 q_2 + \nu_2 p_2 - \gamma_{21} p_2 \left(p_1^2 + q_1^2\right) - \gamma_{22} p_2 \left(p_2^2 + q_2^2\right) + \delta_2 p_1 \left(3 q_1^2 - p_1^2\right). \end{aligned} \tag{17}$$

5. RESULTS AND DISCUSSION

For the analysis of the rotating beam subjected to principal parametric resonance of the first mode (i.e., $\varpi \cong \omega_1$) in presence of 3:1 internal resonance, system parameters are taken as mentioned earlier corresponding to the commensurable natural frequencies of the first and second mode of the system. There are no modal interactions involving other modes. The beam geometrical characteristics used in this analysis are the same employed by others authors (Fazelzadeh and Hosseini, 2007): L = 1.2 m, h = 0.0827 m, b = 0.257 m, e = 0.01654 m and R_0= 1.3 m. The closed box beam is constructed with a metallic alloy (Ti6Al4V) and a ceramic (ZrO2), whose properties are given in Table 1.

Table 1. Temperature depend coefficients of material properties for ceramic (ZrO_2) and metals (Ti-6Al-4V).

	Material	P_{-1}	P_0	P_1	P_2	P_3
E (Pa)	Ti-6Al-4V	0	122.7 x 10^9	-4.605 x 10^{-4}	0	0
	ZrO_2	0	132.2 x 10^9	-3.805 x 10^{-4}	-6.127 x 10^{-8}	0
v	Ti-6Al-4V	0	0.2888	1.108 x 10^{-4}	0	0
	ZrO_2	0	0.3330	0	0	0
ρ (kg/m^3)	Ti-6Al-4V	0	4420	0	0	0
	ZrO_2	0	3657	0	0	0
α (1/K)	Ti-6Al-4V	0	7.43 x 10^{-6}	7.483 x 10^{-4}	-3.621 x 10^{-7}	0
	ZrO_2	0	13.3 x 10^{-6}	-1.421 x 10^{-3}	9.549 x 10^{-7}	0
k (W/mK)	Ti-6Al-4V	0	6.10	0	0	0
	ZrO_2	0	1.78	0	0	0

For a volume fraction exponent K = 1 and T_C = 600 K, the internal resonance is perfectly tuned when $\bar{\Omega}$ = 4.607. The following dimensionless parameter has been considered in the numerical simulations

$$\bar{\omega}_i^2 = \omega_i^2 \frac{\rho A}{EI} L^4 . \tag{18}$$

where ω_i is the ith natural frequency of the beam obtained from Eq. (18). The second natural frequency and three times the first natural frequency are plotted as functions of $\bar{\Omega}$ in Fig. 2. The scaled natural frequencies for a rotating speed $\bar{\Omega}$ = 4.607 are $\bar{\omega}_1$ = 8.9 and $\bar{\omega}_2$ = 26.7. The corresponding nonlinear interaction coefficients (defined in Eq. 17), for the specified rotating speed are: γ_{11} = 15.40, γ_{12} = 1353.19, γ_{21} = -176.485, γ_{22} = -2780.57, δ_1 = -135.43 and δ_2 = 5.56.

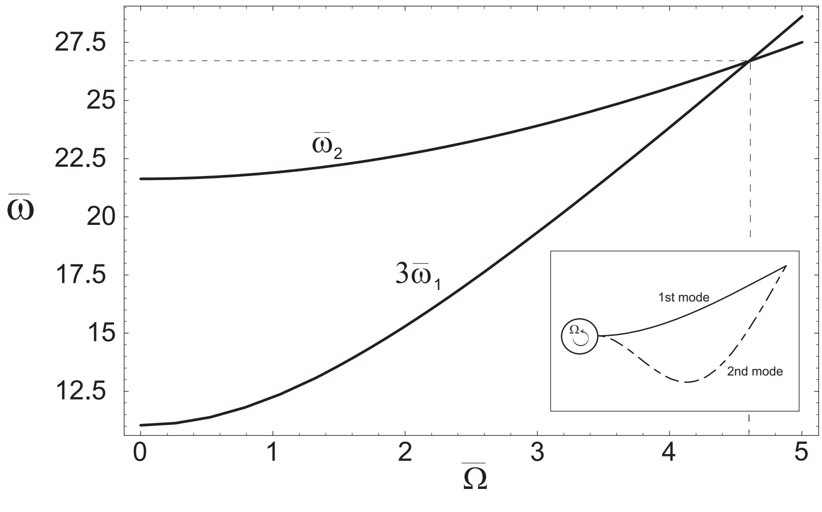

Figure 2. Variations of three times the first $\bar{\omega}_1$ and second $\bar{\omega}_2$ scaled natural frequencies with $\bar{\Omega}$.

5.1 Steady-state motions and stability

The equilibrium solutions of Eq. (17) correspond to periodic motions of the beam. Steady-state solutions are determined by zeroing $p_i' = q_i' = 0$ the right-hand members of the modulation Eq. (17) and solving the non-linear system.

Stability analysis is then performed by analyzing the eigenvalues of the Jacobian matrix of the non-linear equations calculated at the fixed points. The amplitudes a_1 and a_2 are obtained by means of the following expression:

$$a_i = \sqrt{p_i^{\,2} + q_i^{\,2}} \qquad i = 1, 2. \tag{19}$$

The frequency-response curves are shown in Figs. 3a and b, for an internal and external resonance condition. The modal amplitude a_i curves are obtained in function of the external detuning parameter σ_2. In this case, the forcing amplitude is f_1 = 0.025, modal damping d_i = 0.05 and internal detuning parameter σ_1= 0.04. The response curve corresponding to the first modal amplitude shows a noticeable hardening-spring type behavior (Fig. 3a). The modal amplitude of the indirectly excited second mode is smaller in comparison with the first mode (Fig. 3b). In Fig. 3, solid (dotted) lines denote stable (unstable) equilibrium solutions and thin solid lines denote unstable foci.

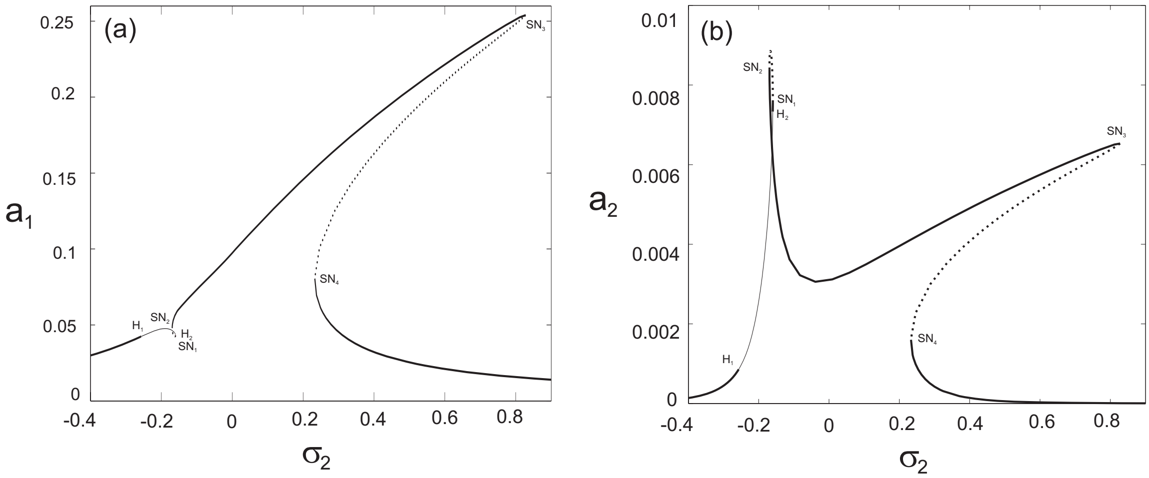

Figure 3. Frequency-response curves for: (a) first and (b) second modes, when f_1 = 0.025, σ_1 = 0.04 and d_i = 0.05. Solid (dotted) lines denote stable (unstable) equilibrium solutions and thin solid lines denote unstable foci.

The response curves exhibit an interesting behavior due to saddle-node bifurcations (where one of the corresponding eigenvalues crosses the imaginary axis along the real axis from the left- to the right-half plane) and Hopf bifurcations (where one pair of complex conjugate eigenvalues crosses the imaginary axis transversely from the left to the right-half plane). As σ_2 increases from a small value, the solution increases in amplitude and loses stability via a Hopf bifurcation at σ_2 = -0.2570 (H_1) and regains its stability via a reverse Hopf bifurcation at σ_2 = -0.1598 (H_2). Then, the response jumps to another branches of stable equilibrium solutions (jump effect), depending on the initial conditions. The dynamics solutions that emerge from this bifurcation will be analyzed in the next section. There is an unstable solution happening between two saddle-node bifurcations SN_1 and SN_2 (σ_2 = -0.1597 and σ_2 = -0.1694). The reduction in amplitude of the first mode represents an increased in the second mode amplitude. Increasing σ_2 beyond SN_2, the stable solution grows again in amplitude until arriving to a saddle-node bifurcation SN_3 (σ_2=0.8279), resulting in a jump of the response to another branches of solutions. The new stable branch is left bounded by a saddle-node bifurcation SN_4 (σ_2 =0.2330).

When the modal damping is reduced d_i = 0.025, the influence of this effect is shown in Figs. 4a and b, conserving the same forcing amplitude and internal detuning parameter values that the previous model. The frequency-response curves are similar to the previous case, and the modal amplitudes are larger. However, it can be seen that the influence of the first mode on the second mode response is smaller in the neighborhood of the Hopf bifurcation H_1 and the saddle-node SN_2.

The influence of the internal detuning parameter on the frequency-response is analyzed in Fig. 5, when the modal damping considered is d_i = 0.05, f_1 = 0.05 and σ_1 is far from the perfect resonance condition. Figures 5a and b shown that when σ_2 increases from a small value, the frequency-response curves seem similar to the previous case. However, for large values of σ_2 the stable equilibrium solution loses stability via a Hopf bifurcation at H_3 and regains its stability via a reverse Hopf bifurcation at H_4.

5.2 Dynamic solutions

According to the Hopf bifurcation theorem, small limit cycles are born as a result of the Hopf bifurcation. The born limit cycles are stable if the bifurcation is supercritical and unstable if the bifurcation is subcritical. Cycle-limit of the modulation equations correspond to aperiodic responses of the beam. In Fig. 6, a bifurcation diagrams for the orbits of the modulation Eq. (17) in the neighborhood of the unstable foci when f_1 = 0.025, σ_1 = 0.04 and d_i = 0.05 (see Fig. 3). The software XPP-AUTO is used to obtain the dynamic solutions that emerge from H_1. Full filled and empty circles denote branches of stable and unstable limit cycles. In addition, we present in Fig. 6 phase portraits in the p_1-p_2 plane characterizing the period-one limit cycles found on each branch. It is observed that a stable small limit cycle born due to the supercritical Hopf bifurcation at H_1 (σ_2 = -0.257). Then, as σ_2 increases, the cycle limit grows and loses stability through a cyclic-fold bifurcation at CF_1 (σ_2 = -0.241). Consequently, the two-period quasiperiod response of the beam jumps to another two-period quasiperiod response. This stable branch is limited to the left and to the right by two cyclic-fold bifurcation CF_2 and CF_3 (σ_2 = -0.2511 and σ_2 = -0.1673, respectively). Increasing σ_2 after CF_3 the dynamic response jumps to a periodic solution.

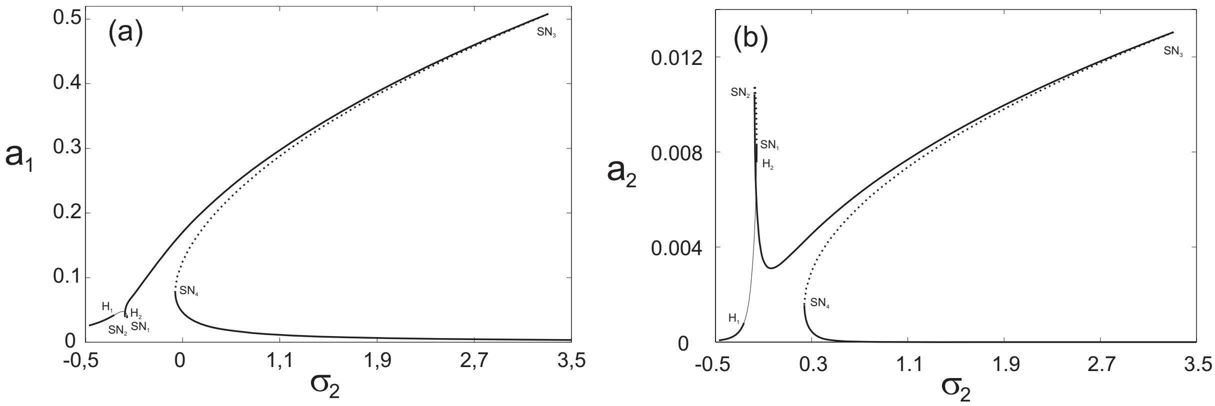

Figure 4. Frequency-response curves for: (a) first and (b) second modes, when f_1 = 0.05, σ_1 = 0.04 and d_i = 0.025. Solid (dotted) lines denote stable (unstable) equilibrium solutions and thin solid lines denote unstable foci.

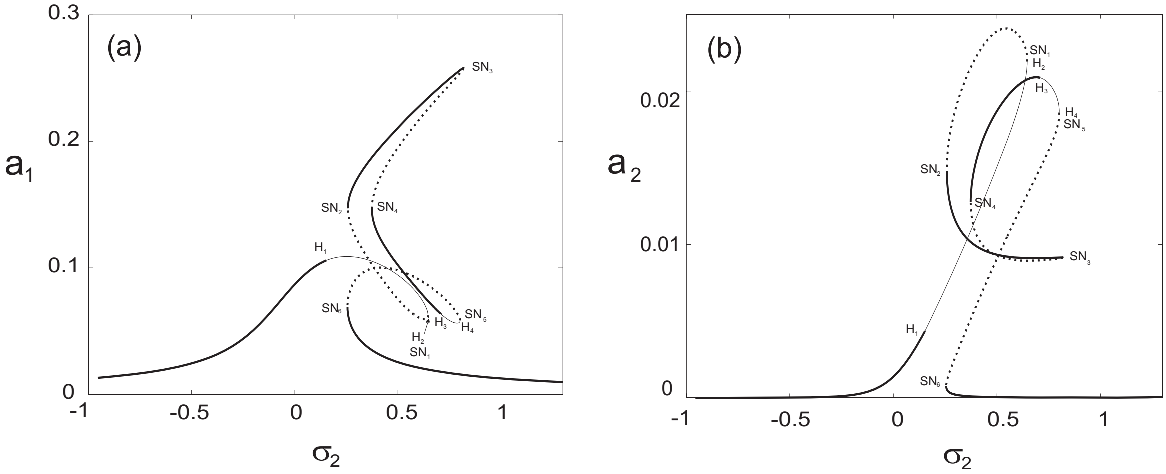

Figure 5. Frequency-response curves for the first and second modes when d_i = 0.05, σ_1 = 4 and f_1 = 0.05. Solid (dotted) lines denote stable (unstable) equilibrium solutions and thin solid lines denote unstable foci.

On the other hand, as σ_2 decreases past the supercritical Hopf bifurcation H_2 (σ_2 = -0.159835), the equilibrium solutions loses stability and gives way to a small-amplitude limit cycle. In Fig. 7, we show a schematic bifurcation diagrams for the orbits of the modulation equations, in the neighborhood of the Hopf bifurcation H_2. As the parameter σ_2 is reduced, the cycle limit grows, as shown in the Figure 8. It then goes through a sequence of cyclic-fold y doubling period bifurcation. When the stable solution encounters a cycle-fold bifurcation, the beam response jumps to a two-period quasiperiodic motion. When σ_2 decreases past *CF* in the last branch (denoted as *VIII* in Fig. 7), the beam response jumps to a periodic solution.

As it was observed in the previous section, the dynamic behavior of the beam becomes more complicated for an internal detuning parameter σ_1 = 4. The dynamic solutions for the case of f_1 = 0.05 and d_i = 0.05 are analyzed (according to the frequency-response curves, Figs. 5a and b). In this case, there are four Hopf bifurcations, where H_1 (σ_2 = 0.04025) and H_3 (σ_2 = 0.756) correspond to supercritical Hopf bifurcation, while H_2 (σ_2 = 0.5667) and H_4 (σ_2 = 0.908) correspond to subcritical Hopf bifurcation. As σ_2 increases from the left Hopf bifurcation H_1, nine branches of solutions are found in the neighborhood of H_1. A schematic diagram of these branches is shown in Fig. 8. It is noticeable that multiple attractors coexist between these branches. The relative sizes of branches of cycles limit in the neighborhood of the Hopf bifurcation H_1 are: 0.04025 < σ_2 < 0.04713 on branch I, 0.06757 < σ_2 <0.06762 on branch II, 0.1528 < σ_2 < 0.1722 on branch III, 0.0447700 < σ_2 < 0.0447733 on branch IV, -0.0148 < σ_2 < -0.013866 on branch V, -0.04594 < σ_2 < -0.04541 on branch VI, -0.07981 < σ_2 < -0.079525 on branch VII, -0.4489 < σ_2 < -0.44818 on branch VIII and -0.8389 < σ_2 < -0.826465 on branch IX.

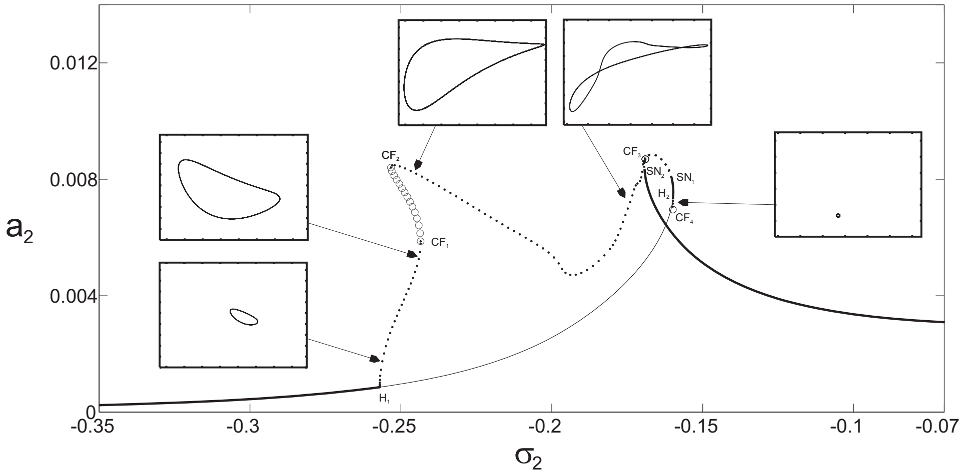

Figure 6. Bifurcation diagrams, which limit cycle encounters between the Hopf bifurcation points when d_i = 0.05, σ_1 =0.04 and f_1 = 0.025. H = Hopf and CF = cycle-fold bifurcation. (•••) Stable limit cycle, (○○○) unstable limit cycle. Solid (dotted) lines denote stable (unstable) equilibrium solutions and thin solid lines denote unstable foci.

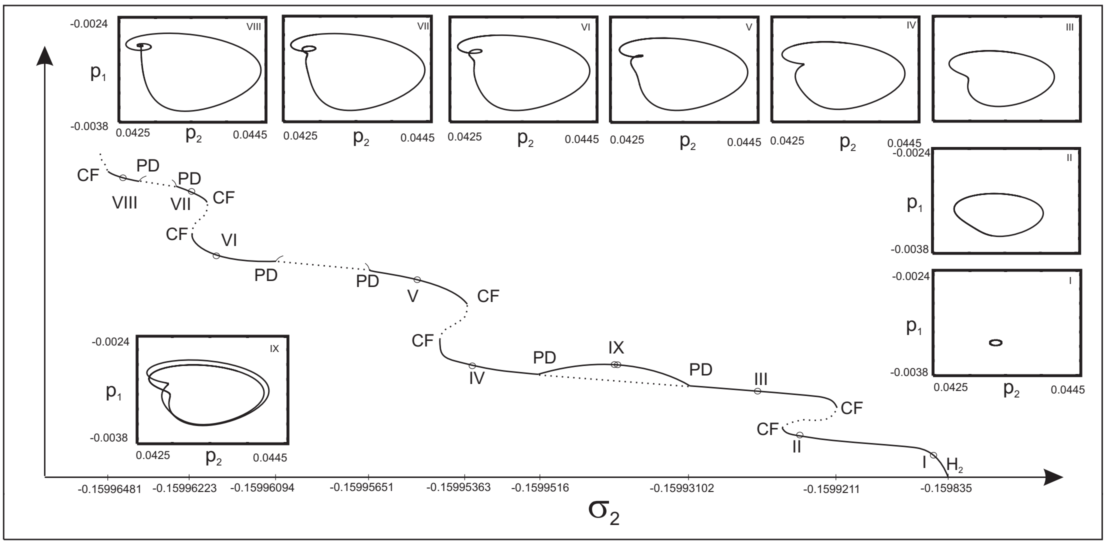

Figure 7. A schematic of the dynamic solutions found in the neighborhood of the Hopf bifurcation H_2, when d_i = 0.05, σ_1 = 0.04 and f_1 =0.025. H = Hopf bifurcation, CF = cycle-fold bifurcation and PD = period-doubling bifurcation. (—) Stable and (···) unstable limit cycles.

In the first branch, a small limit cycle born as a result of the supercritical Hopf bifurcation H_1. Two-dimensional projections of the phase portraits of the limit cycle onto the p_1-p_2 plane at various pre and post-period-doubling bifurcation points are shown in Figures 10a-f. The period-one limit cycle (Figures 10a and b) grows and deforms and remains stable until a period-doubling bifurcation occurs PD_2 (σ_2 = 0.0462763). Then it undergoes a sequence of period doubling bifurcations DP_4 (σ_2 = 0.0470266), DP_8 (σ_2 = 0.0471067), DP_{16} (σ_2 = 0.04713062), culminating in a chaotic attractor as shown in Fig. 11a (σ_2 = 0.04718). As σ_2 increases slightly, the chaotic attractor increases in size and collides with its basin boundary, resulting in the destruction of the chaotic attractor and its basin boundary in a boundary crisis. As a result, the beam response jumps to a far away attractor, as it can be seen in the time history of p_1 in Fig. 11b. Two-dimensional projection of the large attractor is shown in Fig. 12c for a σ_2 = 0.19. Then, as σ_2 is increased further, the large chaotic attractor undergoes a boundary crisis and tends to a periodic solution in the neighborhood of SN_2 (σ_2 = 0.0193, see Figure 9).

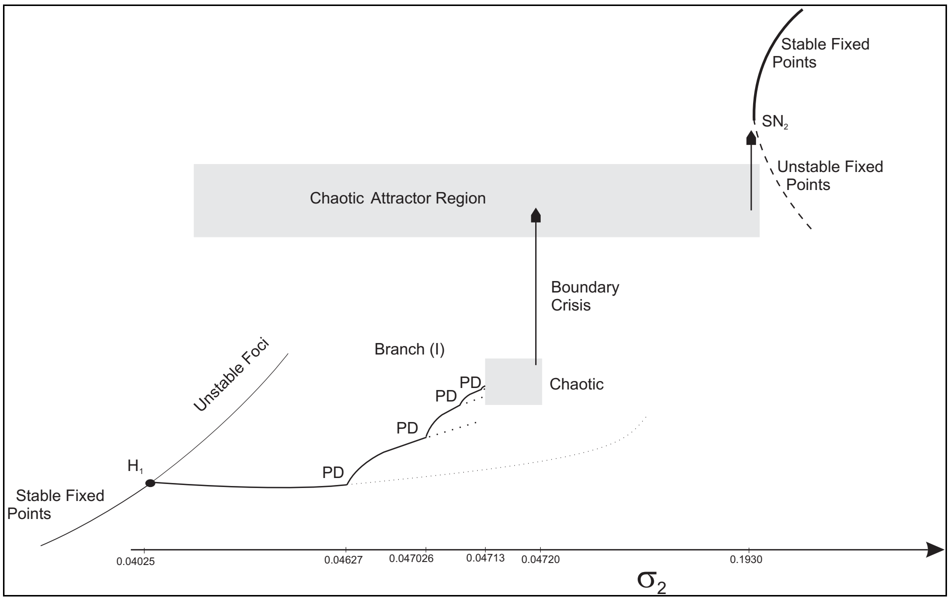

Figure 9. A schematic of the dynamic solutions of branches I found in the neighborhood of the Hopf bifurcation H_1, when d_i = 0.05, σ_1 = 4 and f_1 =0.05. H = Hopf bifurcation, CF = cycle-fold bifurcation and PD = period-doubling bifurcation. (—) Stable and (···) unstable limit cycles.

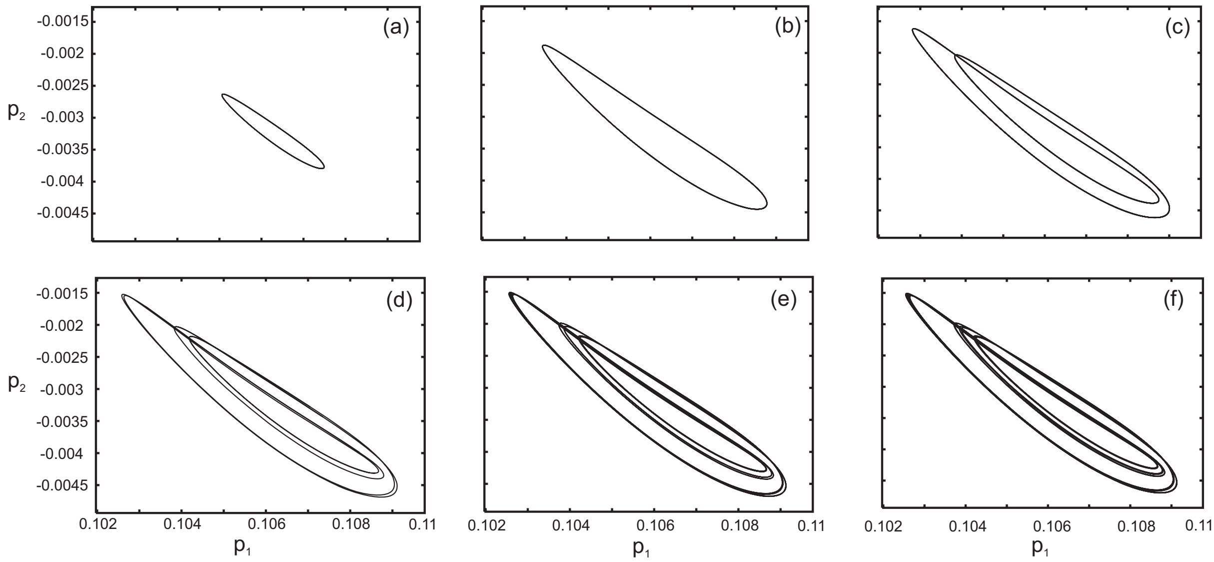

Figure 10. Two-dimensional projections of the phase portraits of the limit cycle found on branch I onto the p_1-p_2 plane, when d_i = 0.05, σ_1 = 4, f_1 =0.05 and σ_2 = (a) 0.04146 (p-1), σ_2 = (b) 0.04592 (p-1), σ_2 = (c) 0.04669 (p-2), σ_2 = (d) 0.04708 (p-4), σ_2 = (e) 0.04712 (p-8) and σ_2 = (f) 0.04713 (p-16).

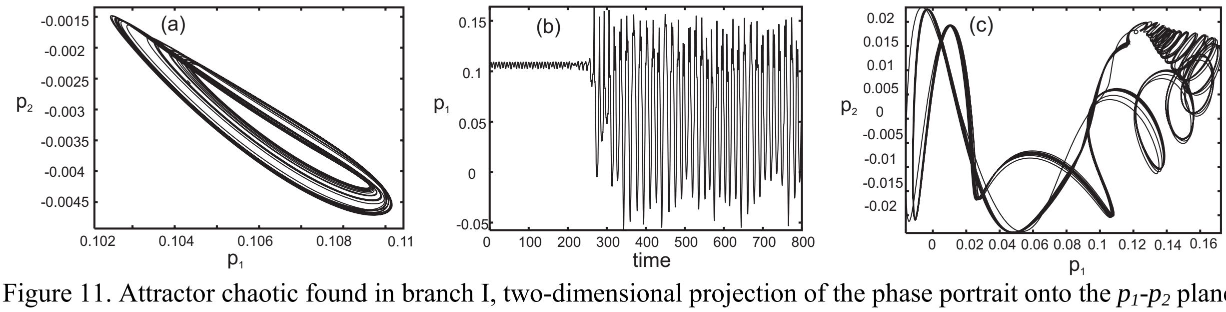

Figure 11. Attractor chaotic found in branch I, two-dimensional projection of the phase portrait onto the p_1-p_2 plane showing the chaotic attractor before and after the explosive bifurcation for (a) σ_2 = 0.0478 and (c) σ_2 = 0.19, and (b) time history of p_1 after a crisis had occurred for σ_2 = 0.0472.

6. CONCLUSIONS

The nonlinear planar response of a cantilever rotating box beam to a principal parametric resonance of its first flexural mode is investigated. The beam is subjected to a harmonic transverse load in the presence of internal resonance. The internal resonance can be activated for a range of the beam rotating speed, where the second natural frequency is approximately three times the first natural frequency. Geometric cubic nonlinear terms are included in the equation of motion due to midline stretching of the beam. The FGMs thermo-mechanical properties vary smoothly and continuously in predetermined directions throughout the body of the structure.

By means of the method of multiple scales applied directly on the partial-differential equation four first-order nonlinear ordinary-differential equations were derived, describing the modulation of the amplitudes and phases of the interacting modes. The resonant behavior is illustrated by frequency-response and amplitude-load curves for a functionally graded materials. The curves are generated using a pseudo arclength continuation scheme. Calculating the eigenvalues of the Jacobian matrix, the stability of these responses is assessed. The frequency-response curves exhibit a hardening type behavior. When the excitation frequency is slowly varied, the response may undergo saddle-node and Hopf bifurcations. On the other hand, when the internal detuning parameter is varied from its perfect condition, the frequency-response curves exhibit a more complex behavior. It was shown that this effect is also influenced by the decrease of the load amplitude parameter value. In this case, it was found that the modulation equations posses complex dynamics, including supercritical period-doubling bifurcation, the coexistence of multiple attractors, and various jump responses driven by cyclic-fold bifurcation, subcritical period-doubling bifurcations, and boundary crises. The limit cycle solutions of the modulation equations may undergo a sequence of period-doubling bifurcations, culminating in chaos. The chaotic attractors may undergo attracting-merging and boundary crises.

7. ACKNOWLEDGEMENTS

The present study was sponsored by Secretaría de Ciencia y Tecnología, Universidad Tecnológica Nacional, and by CONICET. The first author also acknowledges the financial support from the Agencia de Promoción Científica y Tecnológica de Argentina, under the project PICT-2007.

8. REFERENCES

Apiwattanalunggarn, P., Shaw, S.W., Pierre, C., and Jiang, D., 2003, "Finite-Element-Based Nonlinear Modal Reduction of a Rotating Beam with Large-Amplitude Motion", Journal of Vibration and Control, Vol. 9, pp. 235.

Fazelzadeh, S.A., Hosseini, M., 2007, "Aerothermoelastic behavior of supersonic rotating thin-walled beams made of functionally graded materials", Journal of fluids and structures, Vol. 23, pp. 1251-1264.

Leissa, A., 1981, "Vibrational aspects of rotating turbomachinery blades", ASME Applied Mechanics Reviews, Vol. 34, pp. 629-635.

Librescu, L., 2006. "Thin-Walled Composite Beams"¸ Ed. Springer, Dordrecht.

Machado, S.P., Filipich, C.P., and Cortínez, V.H., 2007. "Parametric vibration of thin-walled composite beams with shear deformation", Journal of Sound andVibration, Vol. 305, pp. 563–581.

Malekzadeh, P. Two-dimensional in-plane free vibrations of functionally graded circular arches with temperature-dependent properties. Composite Structures, 91(1) (2010) 38-47.

Nayfeh, A.H., and Mook, D.T., 1979. "Nonlinear Oscillations", Ed. Wiley, New York.

Nayfeh, A.H., 1996. "Nonlinear Interactions", Ed. Wiley, New York, 473p.

Pesheck, E., Pierre, C., and Shaw, S.W., 2002a. "Modal reduction of a nonlinear rotating beam through nonlinear normal modes", ASME Journal of Vibration and Acoustics, Vol. 124, pp. 229–236.

Pesheck, E., Pierre, C., and Shaw, S.W., 2002b. "A new Galerkin-based approach for accurate nonlinear normal modes through invariant manifolds", Journal of Sound and Vibration, Vol. 249, pp. 971–993.

Reddy, J.N., Chin, C.D., 1998. "Thermomechanical analysis of functionally graded cylinders and plates", Journal of Thermal Stresses, Vol. 26, pp. 593-626.

Schilhansl, M.J., 1958. "Bending frequency of a rotating cantilever beam", Journal of Applied Mechanics, Vol. 25, pp. 28-30.

Tanigawa, Y., 1995. "Some basic thermoelastic problems for nonhomogeneous structural materials", Applied Mechanics Review, Vol. 48, pp. 287-300.

Turhan, O., and Bulut, G., 2009. "On nonlinear vibrations of a rotating beam", Journal of Sound and Vibration, Vol. 322, pp. 314–335.

Zhao, F.Q., Wang, Z.M., Liu, H.Z., 2007. "Thermal post-buckling analyses of functionally graded material rod", Applied Mathematics and Mechanics, Vol. 28, pp. 59-67.

9. RESPONSIBILITY NOTICE

The authors are the only responsible for the printed material included in this paper.